

Research Paper

Active Tumor Permeation and Uptake of Surface Charge-Switchable Theranostic Nanoparticles for Imaging-Guided Photothermal/Chemo Combinatorial Therapy

Chia-Chian Hung¹, Wen-Chia Huang¹, Yi-Wen Lin¹, Ting-Wei Yu¹, Hsin-Hung Chen², Sung-Chyr Lin², Wen-Hsuan Chiang^{1,✉} and Hsin-Cheng Chiu^{1,✉}

1. Department of Biomedical Engineering and Environmental Sciences, National Tsing Hua University, Hsinchu 30013, Taiwan
2. Department of Chemical Engineering, National Chung Hsing University, Taichung 402, Taiwan

✉ Corresponding authors: Hsin-Cheng Chiu, Ph.D., Department of Biomedical Engineering and Environmental Sciences, National Tsing Hua University, 101, Section 2, Kuang-Fu Road, Hsinchu 30013, Taiwan. Tel: (886-3-5715131 ext. 34233) E-mail: hscchiu@mx.nthu.edu.tw. Wen-Hsuan Chiang, Ph.D. Department of Biomedical Engineering and Environmental Sciences, National Tsing Hua University, 101, Section 2, Kuang-Fu Road, Hsinchu 30013, Taiwan. Tel: (886-3-5715131 ext. 35494) Email: poemt5637@hotmail.com

© Ivyspring International Publisher. Reproduction is permitted for personal, noncommercial use, provided that the article is in whole, unmodified, and properly cited. See <http://ivyspring.com/terms> for terms and conditions.

Received: 2015.08.29; Accepted: 2015.10.29; Published: 2016.01.01

Abstract

To significantly promote tumor uptake and penetration of therapeutics, a nanovehicle system comprising poly(lactic-co-glycolic acid) (PLGA) as the hydrophobic cores coated with pH-responsive N-acetyl histidine modified D- α -tocopheryl polyethylene glycol succinate (NACHis-TPGS) is developed in this work. The nanocarriers with switchable surface charges in response to tumor extracellular acidity (pH_e) were capable of selectively co-delivering indocyanine green (ICG), a photothermal agent, and doxorubicin (DOX), a chemotherapy drug, to tumor sites. The *in vitro* cellular uptake of ICG/DOX-loaded nanoparticles by cancer cells and macrophages was significantly promoted in weak acidic environments due to the increased protonation of the NACHis moieties. The results of *in vivo* and *ex vivo* biodistribution studies demonstrated that upon intravenous injection the theranostic nanoparticles were substantially accumulated in TRAMP-C1 solid tumor of tumor-bearing mice. Immunohistochemical examination of tumor sections confirmed the active permeation of the nanoparticles into deep tumor hypoxia due to their small size, pH_e -induced near neutral surface, and the additional hitchhiking transport via tumor-associated macrophages. The prominent imaging-guided photothermal therapy of ICG/DOX-loaded nanoparticles after tumor accumulation induced extensive tumor tissue/vessel ablation, which further promoted their extravasation and DOX tumor permeation, thus effectively suppressing tumor growth.

Key words: surface charge transition, deep tumor penetration, tumor hypoxia, photothermal therapy, chemotherapy

Introduction

Aiming at improving efficacy of cancer therapy by effective tumor accumulation of therapeutic agents via the intrinsic enhanced permeability and retention (EPR) effect of solid tumors, various nanoparticle-based drug delivery systems (DDS) have been developed for the last two decades [1-8]. Despite the significant progresses in nanomedicine for targeted drug and bioimaging delivery, drawbacks including

short blood circulation time, low drug bioavailability, and poor tumor penetration/uptake still severely limit the translation of these developments into clinic applications [9-11]. It has been recently demonstrated that coating hydrophilic poly(ethylene glycol) (PEG) and zwitterionic materials on the surfaces of nanocarriers can efficiently increase drug residence in blood circulation and thus tumor accumulation [12-16].

However, such modifications could impede the uptake of nanocarriers by cancer cells [12,13,15,16]. Although it has shown that positively surface-charged nanoparticles exhibited promoted uptake by cancer cells via electrostatic attractions, their application for drug delivery faces challenges because of their rapid body elimination, tissue toxicity and reduced tumor penetration [17,18]. Taking these facts into consideration, it is thus necessary to develop smart DDS that can elude non-specific protein adsorption during blood circulation, yet can actively be transformed into a more cell-interactive structure once localized and accumulated in tumor tissues.

To this end, new strategies of engineering nano-scaled DDS with the capability of transforming surface charges from negative to neutral/positive in response to tumor extracellular acidity (pH_e 6.0~7.0) have emerged [19-25]. Wang and co-workers developed a 2,3-dimethylmaleic anhydride (DMA)-modified nanogel with tumor acidity-activated charge conversion ability as a doxorubicin (DOX) carrier [19]. Through the cleavage of the amide linkages between amine and DMA moieties under weak acidic conditions, the significant increase in surface positive charge enhanced cellular uptake of DOX-loaded nanogels and the cytotoxicity against cancer cells. Also, they exploited the similar concept to attain surface charge switchable nanoparticles based on zwitterionic polymers for improved transport of DOX to tumors [20]. As reported by Bae's group [21], the surface positive charges of paclitaxel (PTX)-carrying cationic micelles shielded by a negatively charged di-block copolymer at physiological pH can be exposed by pH_e -triggered detachment of the surface copolymer, giving the unshielded PTX-loaded micelles a considerably enhanced tumor penetration and antitumor efficacy on MCF-7 tumor-bearing mice. In order to target tumor hypoxia, on the other hand, Dreaden et al. found that the tumor acidity-responsive hyaluronan nanoparticles, prepared by the layer-by-layer (LbL) electrostatic assembly technique, could undergo hypoxic pH-induced structural reorganization that exposed surface positive charges, leading to remarkable enhancement in tumor accumulation and penetration [22]. Distinct from the aforementioned nanocarriers requiring time-consuming hydrolysis and detachment of the shielding materials, Zhang et al. have developed polymeric micelles featuring morpholino-rich surfaces that exhibit a rapid surface charge conversion at pH ranging from 7.0 to 6.5 via protonation of morpholino residues [23].

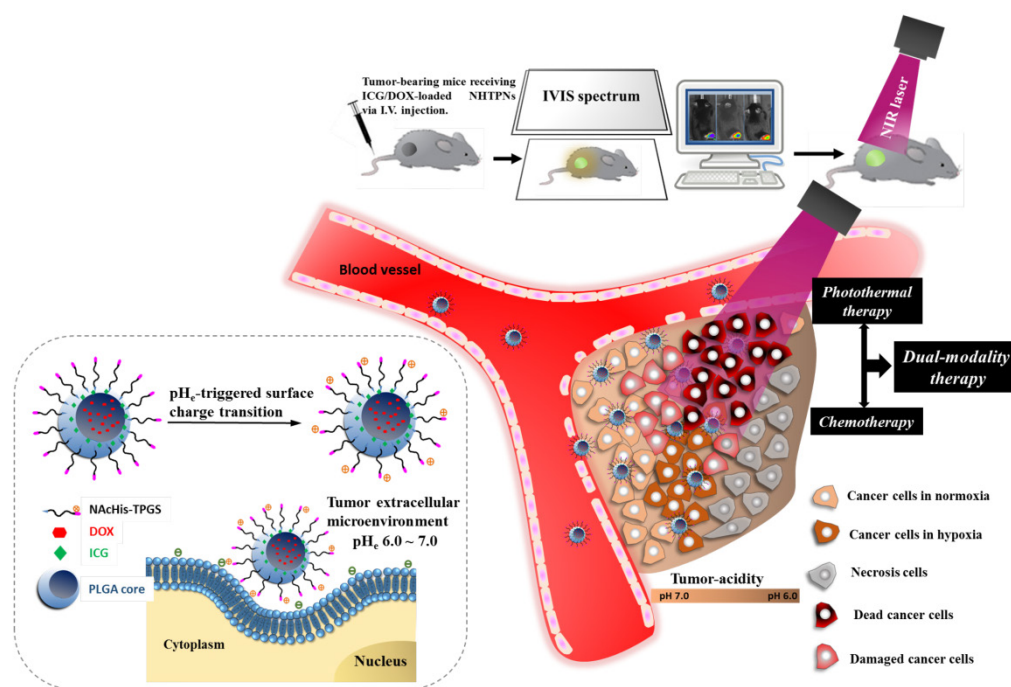
The preparation of these DDS with pH_e -responsive surface charge transition, neverthe-

less, frequently involves the use of complicate materials, excess organic solvents and multi-step procedures. In addition, most of these nanovehicles transport only a single chemotherapy with limited efficacy [19-21, 23, 25-28]. In order to enhance anti-tumor effect by the imaging-guided photothermal/chemo combined therapy, a practical approach was developed herein to prepare pH_e -responsive surface charge-switchable nanoparticles capable of co-delivering a photothermal agent, indocyanine green (ICG), and a chemotherapy drug, DOX (Scheme 1). N-Acetyl histidine (NACHis) modified D- α -tocopheryl polyethylene glycol 1000 succinate (TPGS) (NACHis-TPGS), prepared by conjugating TPGS with NACHis, was anchored via the hydrophobic vitamin E moiety at the surfaces of poly(lactic-co-glycolic acid) (PLGA)-based core particles concomitantly loaded with ICG and DOX. Through the small size (ca. 50 nm) in combination with the increase in surface positive charges due to the pH_e -triggered protonation of NACHis residues [29], the payload-carrying nanoparticles rapidly accumulated in acidic tumor tissues *in vivo* and penetrated into the deep tumor hypoxia regions upon the enhanced uptakes by both TRAMP-C1 cancer cells and tumor-associated macrophages (TAMs). Notably, the imaging-guided near-infrared (NIR)-triggered hyperthermia of the therapeutic nanoparticles accumulated at tumor sites in conjunction with chemotherapy efficiently inhibited tumor growth and recurrence, suggesting that the pH_e -sensitive nanovehicles developed in this work are promising in advanced cancer theranostic applications.

Materials and Methods

Materials

PLGA (LA/GA 85/15, I.V. 0.42 dl/g, hydroxyl terminated) was acquired from Green Square (Taiwan). TPGS, N,N'-dicyclohexylcarbodiimide (DCC), 4-dimethylaminopyridine (DMAP) and 3-(4,5-Dimethylthiazol-2-yl)-2,5-diphenyltetrazolium bromide (MTT) were supplied by Sigma-Aldrich (USA). NACHis was purchased from Tokyo Chemical (Japan). DOX in HCl salt form was obtained from Seedchem (Australia) and ICG from Chem-Impex International (USA). Dulbecco's modified Eagle medium (DMEM), 4',6-Diamidino-2-Phenylindole (DAPI), Hoechst 33342, Alexa Fluor® 488, anti-mouse CD31 antibody, anti-HIF1 α -fluorescein and rat anti-mouse CD11b antibody were purchased from Invitrogen (USA). Deionized water was produced from Milli-Q Synthesis (18 M Ω , Millipore). All other chemicals were reagent grade and used as received.



Scheme 1. Illustration of active tumor penetration and uptake of dual drug-loaded nanoparticles with pH_e-triggered surface charge transition for the imaging-guided photothermal/chemo combinatorial therapy.

Synthesis of NAcHis-TPGS

TPGS (3 g, 2.0 mmol), NAcHis (1.97g, 10.0 mmol), DCC (1.24 g, 6.0 mmol) and DMAP (0.24 g, 2.0 mmol) were dissolved in anhydrous DMSO (10.0 mL). The reaction was carried out under stirring at 40 °C for 48 h, followed by repeated filtrations to remove the byproduct dicyclohexylcarbodiurea. The solution was then dialyzed (Cellu Sep MWCO 1000) against deionized water for 7 days to eliminate the residual NAcHis, DMAP and DMSO. The final product was obtained by lyophilization.

Preparation of Nanoparticles

To obtain hydrophobic DOX in free base form, DOX hydrochloride was stirred in dark overnight with excess triethylamine (1.5-fold excess in molar concentration with respect to DOX) in dry DMSO. Various cargo-loaded nanoparticles coated with either TPGS or NAcHis-TPGS were attained by the one-step nanoprecipitation approach. The NAcHis-TPGS/PLGA nanoparticles (denoted hereinafter as NHTPNs) loaded with ICG and DOX were attained as follows. PLGA (2.0 mg), DOX (0.4 mg) and ICG (0.4 mg) dissolved in DMSO (0.4 mL) were added dropwise into the pH 7.4 phosphate buffer (10 mM, 3.5 mL) containing NAcHis-TPGS (1.6 mg). The solution was stirred at 30 °C for 30 min, followed by an equilibration period of 30 min. The solution containing cargo-loaded NHTPNs was dialysed (Cellu Sep MWCO 12000-14000) against 10 mM pH 7.4 phosphate buffer at 4 °C to remove the residual DOX and

ICG. For comparison, ICG-loaded, DOX-loaded and drug-free NHTPNs, ICG/DOX-loaded TPGS/PLGA nanoparticles (TPNs) without NAcHis conjugation, and ICG/DOX-loaded PLGA nanoparticles (PNs) were prepared in a similar manner.

Characterization of Nanoparticles

The particle size, size distribution and zeta potential of cargo-loaded nanoparticles in aqueous solutions were determined by dynamic light scattering (DLS) using a ZetaSizer Nano Series instrument (Malvern Instruments, U.K.). The data shown herein represented an average of at least triplicate measurements. The morphology of pristine and cargo-loaded nanoparticles was examined by transmission electron microscopy (TEM) (HT7700, Hitachi, Japan) after negative staining with uranyl acetate. The absorption spectra of free ICG and ICG-carrying nanoparticles in PBS were attained using a UV/Vis spectrophotometer (U2900, Hitachi, Japan).

To quantify ICG and DOX loaded within nanoparticles, a prescribed volume of cargo-containing nanoparticle solution was freeze-dried and then dissolved in DMSO for complete particle disruption and payload release. The absorbance of ICG at 775 nm and the DOX fluorescence in the range 500-700 nm were determined, respectively, by a UV/Vis spectrophotometer and a fluorescence spectrometer (F-7500, Hitachi, Japan). The drug loading efficiency (DLE) and loading content (DLC) were calculated by the following formulas:

DLE (%) = (weight of drug loaded/weight of drug in feed) \times 100%.

DLC (%) = (weight of drug loaded/total weight of drug-loaded nanoparticles) \times 100%.

Various ICG-containing nanoparticles and free ICG species in PBS (1.0 mL) were irradiated with 808 nm NIR laser (1.0 W/cm²) for 10 min. The solution temperatures and infrared thermographic maps were recorded using an infrared thermal imaging camera (Thermo Shot F20, NEC Avio Infrared Technologies, Germany).

For ICG release measurement, the ICG-containing nanoparticle solution (2.0 mL) was dialyzed (Cellu Sep MWCO 12000-14000) against PBS (pH 7.4, 40 mL) at 37 °C. The internal sample was withdrawn periodically and the absorbance at 775 nm was determined. The sample solution was placed back into the dialysis tube after each analysis. The cumulative ICG release (%) was calculated by the following equation:

Cumulative ICG release (%) = ((Initial ICG absorbance - ICG absorbance at the predetermined time points)/Initial ICG absorbance) \times 100%.

For DOX liberation evaluation, the DOX-containing nanoparticle dispersion (1.5 mL) was dialyzed (Cellu Sep MWCO 12000-14000) against PBS (pH 7.4, 40 mL) and succinic acid buffer (pH 6.0, 40 mL) at 37 °C, respectively. At the prescribed time intervals, 0.7 mL of dialysate (pH 6.0 or 7.4) was taken for analysis and replaced with an equal volume of fresh buffer. The amount of DOX released was determined by fluorescence measurements.

In Vitro Cellular Uptake

Free ICG, free DOX, ICG/DOX-loaded NHTPNs and TPNs were dispersed in DMEM of different pH values (7.4, 6.6 and 6.3) to an ICG or DOX concentration of 20 μ M. The mouse prostate cancer cells, TRAMP-C1, seeded at a density of 3×10^5 cells per well in 12-well culture plates were incubated with the above solutions at 37 °C for 2 h and then washed three times with PBS. DMSO (0.65 mL) was added for cell disruption. The collection of fluorescence signals of ICG (Ex. 745 nm and Em. 810 nm) was conducted on an IVIS (Xenogen IVIS Spectrum). The amount of DOX uptaken by TRAMP-C1 cells was determined by fluorescence measurements. The FACSCalibur flow cytometer (BD Bioscience) was utilized to assess cellular uptake of ICG/DOX-loaded NHTPNs and TPNs (DOX concentration = 20 μ M) by TRAMP-C1 cells at 37 °C and at pH 7.4 and 6.3. After 2 h incubation, the treated TRAMP-C1 cells (3×10^5 cells/well) were detached with trypsin-EDTA solution and then suspended in PBS (1.0 mL), giving a cell suspension

containing a minimum of 1×10^4 cells. On the other hand, TRAMP-C1 cells (3×10^5 cells/well) seeded onto 22 mm round glass coverslips in 6-well plates were incubated with free DOX, ICG/DOX-loaded NHTPNs and TPNs (DOX concentration = 10 μ M) at pH 7.4 and 6.3 for 1.5 h. After being washed twice with PBS and immobilized with 4 % formaldehyde, the cell nucleus and F-actin of cytoskeleton were stained with Hoechst 33342 and CytoPainter F-actin Staining Kit-Green Fluorescence, respectively. The cellular images were attained using a Nikon ECLIPSE Ti-U inverted microscope (Japan) equipped with a Hoechst set (Ex. 360 nm and Em. 461 nm), an Alexa Fluor 488® Phalloidin set (Ex. 495 nm and Em. 518 nm) and a DOX set (Ex. 488 nm and Em. 590 nm)

In Vitro Photothermal Effects

TRAMP-C1 cells (1×10^5 cells/well) were seeded in a 24-well plate and incubated in DMEM containing 10% FBS and 1% penicillin at 37 °C for 24 h. The spent medium was then replaced with 1.0 mL of fresh DMEM containing free ICG, free DOX or various nanoformulations and was further incubated for additional 24 h. After being washed twice with PBS, cells were detached with trypsin-EDTA and centrifuged. The cell pellets thus collected were dispersed in DMEM (20 μ L) and the dispersion was irradiated with 808 nm NIR laser (1.0 W/cm²) for 5 min. The laser-treated cells were reseeded in a 96-well plate and re-incubated for 24 h. MTT (0.25 mg/mL, 200 μ L) was then added into each well, followed by incubation at 37 °C for 4 h. After discarding the culture medium, DMSO (200 μ L) was added to dissolve the precipitate and the resulting solution was measured for absorbance at 570 nm using a SpectraMax M5 microplate reader. The viability of TRAMP-C1 cells treated with different nanoformulations without NIR laser irradiation was evaluated in a similar manner.

Animals and Tumor Model

Male C57BL/6J mice (6~8 weeks old), purchased from National Laboratory Animal Center (Taiwan), were cared in accordance with the Guidance Suggestions for the Care and Use of Laboratory Animals, approved by the Administrative Committee on Animal Research in the National Tsing Hua University (Taiwan). To establish tumor model, 2×10^7 TRAMP-C1 cells were subcutaneously injected into the right thigh of mice. Two weeks post-inoculation, the low permeability tumor model was established. Tumor volume (V) was calculated as follows: $V = L \times W^2/2$, where W is the tumor measurement at the widest point and L the tumor dimension at the longest point.

In Vivo Imaging and Biodistribution

When the tumor volume reached 100~120 mm³, PBS, free ICG, or various nanoformulations were injected into the mice via tail vein at an ICG dosage of 1.6 mg/kg. The fluorescence signals of ICG (Ex. 745 nm and Em. 810 nm) at 2, 4, 6, 24 and 48 h post-injection were collected on the IVIS. The treated mice were then sacrificed and the major organs harvested for individual organ imaging by IVIS.

Intratumoral Distribution of Therapeutic Nanoparticles

The tumor-bearing mice receiving free DOX, ICG/DOX-loaded NHTPNs and TPNs with and without NIR irradiation were sacrificed 48 h post-injection. The tumors were harvested and stored for cryo-section. Rat anti-mouse CD31, anti-hypoxia-inducible factor (HIF) 1 α and rat anti-mouse CD11b, and, with Alexa Fluor 488[®] goat anti-rat as the secondary antibody, were used for the immunohistochemical (IHC) identifications of tumor neovessel, hypoxia and TAM, respectively, in the cryo-sections. The cell nuclei were stained with DAPI. All stained tumor sections were examined by Nikon ECLIPSE Ti-U inverted microscope with the fluorescence channels for DAPI, Alexa Fluor 488 and DOX.

In Vivo Temperature Measurements upon NIR Irradiation

The protocol for the in vivo distribution studies was followed, with the exception that the tumor site of mice was irradiated with 808 nm laser with a power density of 1.0 W/cm² for 5 min at 6 h post-injection. The tumor local temperature was monitored by infrared thermal imaging camera.

In Vivo Tumor Growth Inhibition

When tumor volume of the mice reached 100~120 mm³, the mice were randomly divided into six groups (10 in each group) and separately treated by I.V. injection with PBS, free ICG, free DOX, ICG-loaded NHTPNs, ICG/DOX-loaded NHTPNs and TPNs at an ICG dosage of 1.6 mg/kg or, in the case of free DOX, 1.8 mg DOX /kg. Six h post-injection, the mice (5 in each group) were irradiated at the tumor sites with 808 nm laser (1.0 W/cm²) for 5 min. The tumor volumes of various groups were measured daily and normalized against the original volumes to assess the antitumor efficacy. The body weight of mice was also monitored daily until 15 days post-injection. The tumors were then isolated from the euthanized mice and weighted for therapeutic index (TI) measurements. The TI defined below was utilized as a quantitative measure of therapeutic efficacy.

$$TI (\%) = \left(1 - \frac{\text{Weight of tumor in the experimental group}}{\text{Weight of tumor in the control group}} \right) \times 100\%$$

Sections of tumors and major organs of pertinent sizes were H&E stained and examined by an Olympus IX70 inverted microscope (Japan).

Statistical Analysis

Data were reported as mean \pm SD. The differences among groups were determined using one-way ANOVA analysis; (*) P < 0.05, (**) P < 0.005 and (***) P < 0.001.

Results and Discussion

Synthesis and Characterization of NAcHis-TPGS

The NAcHis-TPGS employed in this study was prepared by the DCC/DMAP mediated esterification of TPGS with NAcHis. The detail synthetic route of NAcHis-TPGS and its ¹H-NMR characterization are illustrated in **Figure S1** (Supplementary Materials). Based on the integral ratio of the feature proton signals of imidazole ring (7.55 ppm) of NAcHis and the methyl groups (0.81 ppm) of TPGS, the coupling efficiency was estimated to be ca 95%. The yield is above 85 %.

Preparations and Characterization of Payload-Carrying PLGA-Based Nanoparticles

The DOX/ICG-loaded nanoparticles coated with either NAcHis-TPGS (NHTPNs) or TPGS (TPNs) exhibited comparable mean hydrodynamic diameters (D_h) of ca 50 nm and mono-modal size distributions (PDI ca 0.11) in aqueous solution (pH 7.4) (**Figure 1a** and **Table 1**). The TEM images further revealed that these nanoparticles were well-dispersed and spherical (**Figure 1b**), indicating that the TPGS adduct retained the amphiphilic property of the parent compound, and thus was able to anchor on the PLGA particles via the hydrophobic vitamin E moieties and to stabilize the nanoparticles in aqueous solution with PEG segments. By contrast, due to the lack of TPGS or its adduct coating on particle surfaces, the resulting ICG/DOX-loaded PNs readily aggregated in aqueous phase as reflected by their enlarged particle size characterized by both DLS (**Figure 1a** and **Table 1**) and TEM (**Figure 1b**). The coating of either TPGS or its NAcHis conjugate on PLGA particles remarkably enhanced the loading efficiencies of ICG and DOX (**Table 1**), most likely because of the association of ICG and DOX, respectively, with the vitamin E moiety of TPGS through either π - π aromatic and hydrophobic alkyl stacking, although the orientation of these molecules on molecular level is currently not clear. This hypothesis was supported by the observation that,

when ICG molecules were incorporated into the nanoparticles coated with TPGS or NAcHis-TPGS, the feature absorption peak of ICG was appreciably shifted from 776 to 794 nm (Figure 1c) by their association with the hydrophobic alkyl chains of TPGS. Similar findings have also been reported elsewhere [30,31].

To evaluate the aqueous photostability of ICG associated with PLGA-based nanoparticles, the change in absorbance of the ICG-containing nanoparticles in PBS (pH 7.4, I = 0.15 M) at 37 °C was monitored. The maximum absorbance of ICG at each time point relative to that at the beginning (Figure 2a) was obtained from the time-evolved absorption spectra, illustrated in Figure S2. While the normalized ab-

sorbance of free ICG decreased considerably over 7 days, only a slight change in absorbance was observed for ICG-containing nanoparticles. The promoted photostability was primarily ascribed to the protective effect of PLGA nanoparticles serving as the ICG dispersion matrices that prevented ICG from rapid self-aggregation and degradation in aqueous phase [30,31]. Distinct from a severe aggregation of ICG/DOX-loaded PNs upon 4-day incubation in PBS, the particle sizes of cargo-carrying NHTPNs and TPNs remained essentially unchanged over a time period of 7 days (Figure 2b). The results further demonstrate the effect of the surface elaboration with TPGS or NAcHis-TPGS on the colloidal stability of PLGA nanoparticles in aqueous phase.

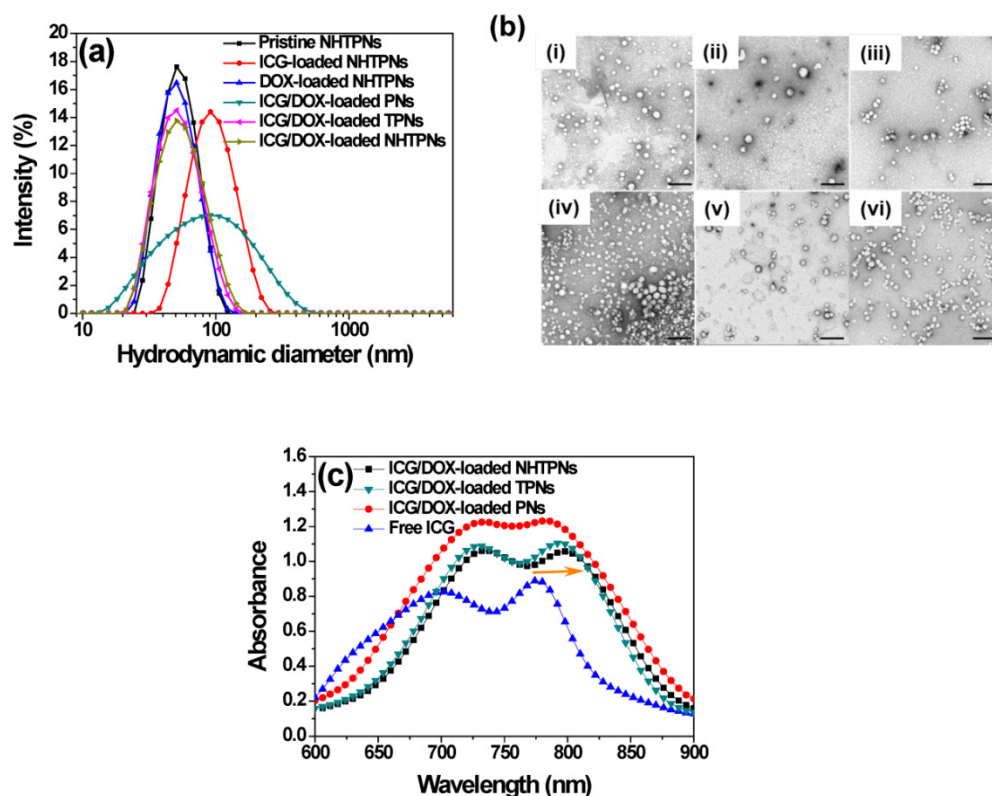


Figure 1. (a) DLS particle size distribution profiles of nanoparticles in aqueous solution of pH 7.4. (b) TEM images of (i) pristine NHTPNs, (ii) ICG-loaded NHTPNs, (iii) DOX-loaded NHTPNs, (iv) ICG/DOX-loaded PNs, (v) ICG/DOX-loaded TPNs and (vi) ICG/DOX-loaded NHTPNs. Scale bars are 200 nm. (c) UV/Vis spectra of free ICG, ICG/DOX-loaded NHTPNs, TPNs and PNs in PBS.

Table 1. DLS Data and Drug Loading Characteristics of Cargo-Loaded Nanoparticles.

Sample	D_h (nm)	PDI	DOX Loading Efficiency (%)	DOX Loading Content (wt %)	ICG Loading Efficiency (%)	ICG Loading Content (wt %)
ICG/DOX-loaded NHTPNs	50.4 ± 2.0	0.116	86.4 ± 3.2	7.5 ± 0.3	77.3 ± 1.7	6.7 ± 0.2
ICG/DOX-loaded TPNs	48.1 ± 1.5	0.112	87.3 ± 2.8	7.6 ± 0.1	76.2 ± 1.3	6.6 ± 0.2
ICG/DOX-loaded PNs	65.1 ± 6.0	0.377	74.2 ± 3.5	10.6 ± 0.2	59.1 ± 2.1	8.4 ± 0.3
ICG-loaded NHTPNs	78.1 ± 3.2	0.102	-	-	70.5 ± 2.4	6.7 ± 0.3
DOX-loaded NHTPNs	49.5 ± 1.2	0.080	88.2 ± 2.8	8.4 ± 0.3	-	-
Pristine NHTPNs	50.2 ± 1.1	0.080	-	-	-	-

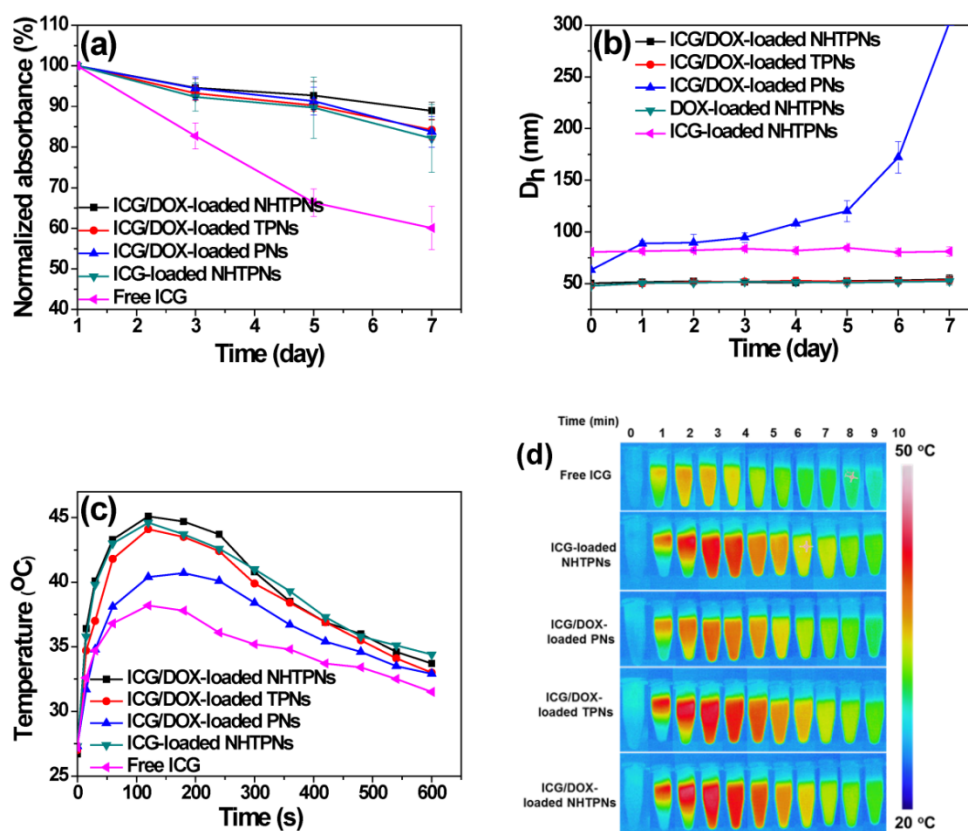


Figure 2. (a) Normalized maximum absorbance of free ICG and various ICG-containing nanoparticles in PBS at 37 °C. (b) Time-evolved mean hydrodynamic diameters (D_h) of various cargo-loaded nanoparticles in PBS at 37 °C. (c) Temperature profiles and (d) thermal images of free ICG and ICG-containing nanoparticles (ICG concentration = 10 μ M) in PBS with 808 nm NIR laser irradiation (1.0 W/cm²).

The NIR-triggered hyperthermia capability of free ICG and ICG-loaded PLGA nanoparticles was examined by monitoring the temperature of the aqueous solution upon receiving laser irradiation at 808 nm. Upon NIR laser irradiation (power density of 1.0 W/cm²) for 120 s, the temperatures of ICG/DOX-carrying NHTPN and TPN solutions were appreciably raised compared with those of the ICG/DOX-loaded PN and free ICG solutions (Figure 2c and d), due largely to the red-shift in the absorption of ICG embedded within NHTPNs and TPNs that better matched the central wavelength (808 nm) of the diode laser used [32]. As expected, the level of temperature increase, a direct measure of NIR-triggered hyperthermia, increased with the concentrations of ICG-loaded NHTPNs and TPNs (Figure S3). The temperatures of all ICG-containing solutions declined gradually 3 min after irradiation due to photo-bleaching and thermal degradation of ICG [32, 33].

pH-Activated Surface Charge Conversion and In Vitro ICG and DOX Release

With the medium pH being adjusted from 7.4 to 5.0, conversions in zeta potentials of pristine and payload-carrying NHTPNs from negative to nearly neutral or slightly positive values were observed

(Figure 3a), due to the enhanced protonation of the imidazole groups of the NAcHis-TPGS segments. By contrast, due to the lack of pH-sensitive moiety in TPGS, no significant variation in the zeta potential of cargo-loaded TPNs in response to pH change was observed. While both the pristine and DOX-loaded NHTPNs became positively charged on their surfaces in response to the pH adjustment to 5.0, the same pH stimulation only rendered the surfaces of NHTPNs carrying either ICG alone or both ICG/DOX nearly neutral, yet still mildly negatively charged, due to the sulfonate groups of ICG present mainly on colloidal surfaces. Most of the DOX species were not involved in charge variations as they remained in free base form, rendering themselves hydrophobic and entrapped within the inner core of NHTPNs (Scheme 1). Notably, the mean particle sizes of the cargo-loaded NHTPNs and TPNs remain essentially invariant in the medium pH range 5.0~7.4, as partly illustrated in Figure 3b. This is particularly important that the ICG/DOX-loaded NHTPNs which exhibit neutral surfaces, maintained a particle size of ca 50 nm in D_h when exposed to the weak acidic environment (pH 6.0) close to p*H*_e (Figure 3b), a critical prerequisite for the infiltration into deep tumor tissue in vivo [34-36].

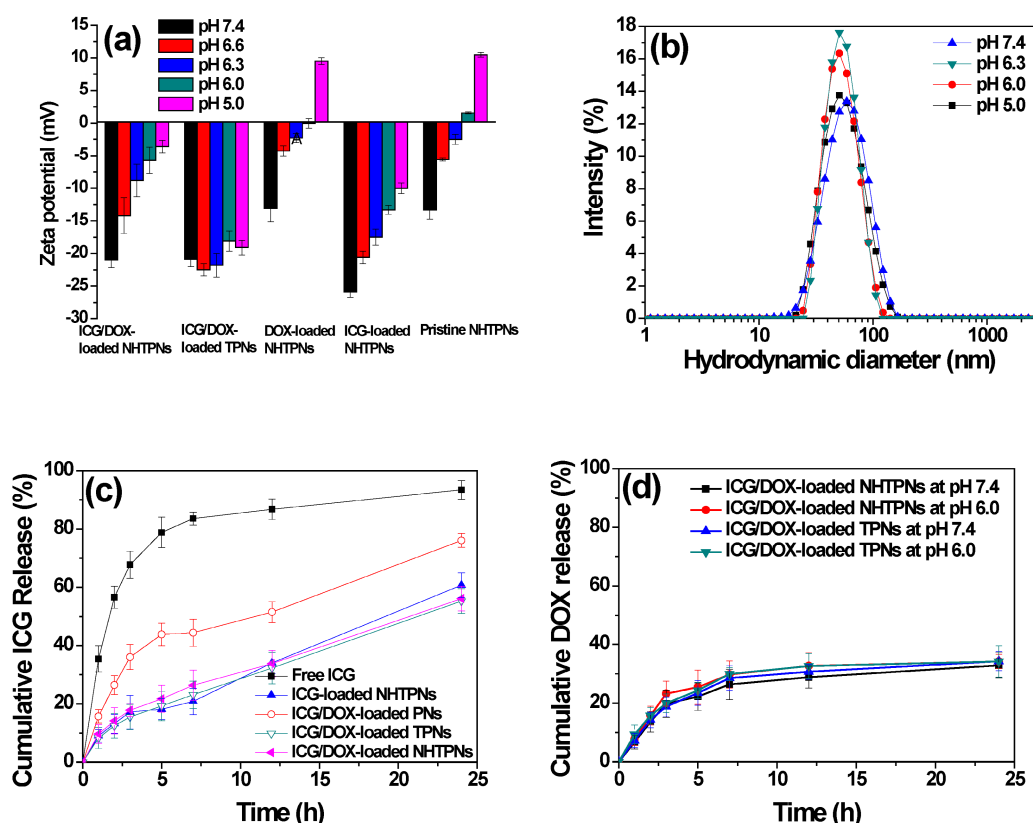


Figure 3. (a) Zeta potential of pristine and cargo-loaded nanoparticles in aqueous solutions. (b) DLS particle size distribution profiles of ICG/DOX-loaded NHTPNs in aqueous solutions. (c) Cumulative ICG release profiles of various cargo-loaded nanoparticles in PBS at 37 °C. (d) Cumulative DOX release profiles of ICG/DOX-loaded NHTPNs and TPNs in aqueous solutions of pH 7.4 and 6.0.

Compared to rapid diffusion of free ICG across the dialysis tube in PBS (>80% over 5 h), the ICG liberation from cargo-loaded nanoparticles under the same conditions was considerably retarded, in particular for those nanoparticles elaborated by TPGS or its NAcHis conjugate (Figure 3c), which can be ascribed to the association of ICG with the vitamin E moiety of TPGS or NAcHis-TPGS on particle surfaces as described above. In contrast to the frequently observed strong pH-dependent release of DOX (in salt form) from pH-responsive polymeric delivery carriers, the DOX release profiles of ICG/DOX-loaded NHTPNs and TPNs were slower and independent of medium pH (Figure 3d), as the hydrophobic DOX was localized primarily within the solid PLGA cores of the nanoparticles. It can thus be presumed that the DOX release profile relied in large measure on the degradation rate of PLGA composing the hydrophobic cores of ICG/DOX-loaded nanoparticles.

In Vitro Tumor Acidity-Mediated Cellular Uptake

The effect of pH-responsive surface charge transition of the cargo-carrying NHTPNs on their cellular uptake was studied using TRAMP-C1 cells as a cell model. When the culture pH was adjusted from 7.4 to

6.3, the NIR fluorescence intensity of ICG molecules from TRAMP-C1 cells treated with ICG/DOX-loaded NHTPNs was significantly enhanced compared with the cancer cells incubated with either ICG/DOX-loaded TPNs or free ICG (Figure 4a). The amount of intracellular DOX of TRAMP-C1 cells incubated with ICG/DOX-loaded NHTPNs was ca 1.5-fold enhanced in response to the pH reduction from 7.4 to 6.3 (Figure 4b), while those of cells treated with either free DOX or ICG/DOX-loaded TPNs were virtually pH independent. The pH-dependent increase in cellular uptake of ICG/DOX-loaded NHTPNs was also confirmed by flow cytometric histograms (Figure 4c). The results strongly suggest that the payload-carrying NHTPNs can effectively promote the intracellular cargo delivery under weak acidic conditions due to the enhanced affinity for cancer cells mediated by the positive charges of NAcHis-TPGS extending into surrounding aqueous phase from the negatively charged surfaces of ICG-embedded PLGA-based nanoparticles. The same findings were attained with another cell model, human breast MCF-7 cancer cells (Figure S4). In agreement with these observations, the fluorescence images show that DOX delivered by NHTPNs at pH 6.3 was found appreciably in the cytoplasm and nuclei of

TRAMP-C1 cells, whereas relatively small amounts of DOX transported by either NHTPNs at pH 7.4 or by TPNs at both pH 7.4 and 6.3 were observed intracellularly (Figure 4d). Compared to ICG/DOX-loaded NHTPNs found largely in cytoplasm and cell nuclei, free hydrophobic DOX molecules were mostly localized within cell membrane (Figure S5), consistent with the observation by Gu's group [37]. In addition, an appreciably higher cellular uptake of free DOX than that of DOX carried by NHTPNs or TPNs at pH 7.4 was observed (Figure 4b). Such differences are resulting mainly from the distinctive cellular uptake pathways for DOX species transported by NHTPNs (endocytosis) and for free DOX molecules (passive diffusion) [6, 37-40].

In Vitro Photothermal/Chemo Combinatorial Therapy

To study the therapeutic efficacy of ICG-based photo-triggered hyperthermia combined with DOX chemotherapy, the viability of TRAMP-C1 cells treated with NHTPNs carrying single- and dual-modality therapy at pH 7.4 was determined by

MTT assay. TRAMP-C1 cells alone exposed to NIR laser irradiation as a control group retained the viability above 95%, being indicative of the harmlessness of NIR laser to cancer cells. While free ICG-treated TRAMP-C1 cells retained a mean viability above 90%, the viability of TRAMP-C1 cells incubated with ICG-loaded NHTPNs was significantly reduced upon NIR activation (Figure 5a), indicating that NIR activation of ICG delivered by NHTPNs displayed strong thermal ablation on TRAMP-C1 cells. This is primarily attributed to the superior photo-triggered hyperthermia ability and photostability of the ICG delivered by NHTPNs in comparison with free ICG (Figure 2). Figure 5a also shows that, at a DOX concentration of 11 μM without NIR irradiation, the ICG/DOX-loaded NHTPNs exhibited higher cytotoxicity against TRAMP-C1 cells (ca 40% cell death) than free DOX (15%), due to the promoted intracellular transport of DOX via endocytic uptake of NHTPNs to cellular nuclei in contrast to the diffusion-based accumulation of free hydrophobic DOX within cell membranes, as shown in Figure 5S.

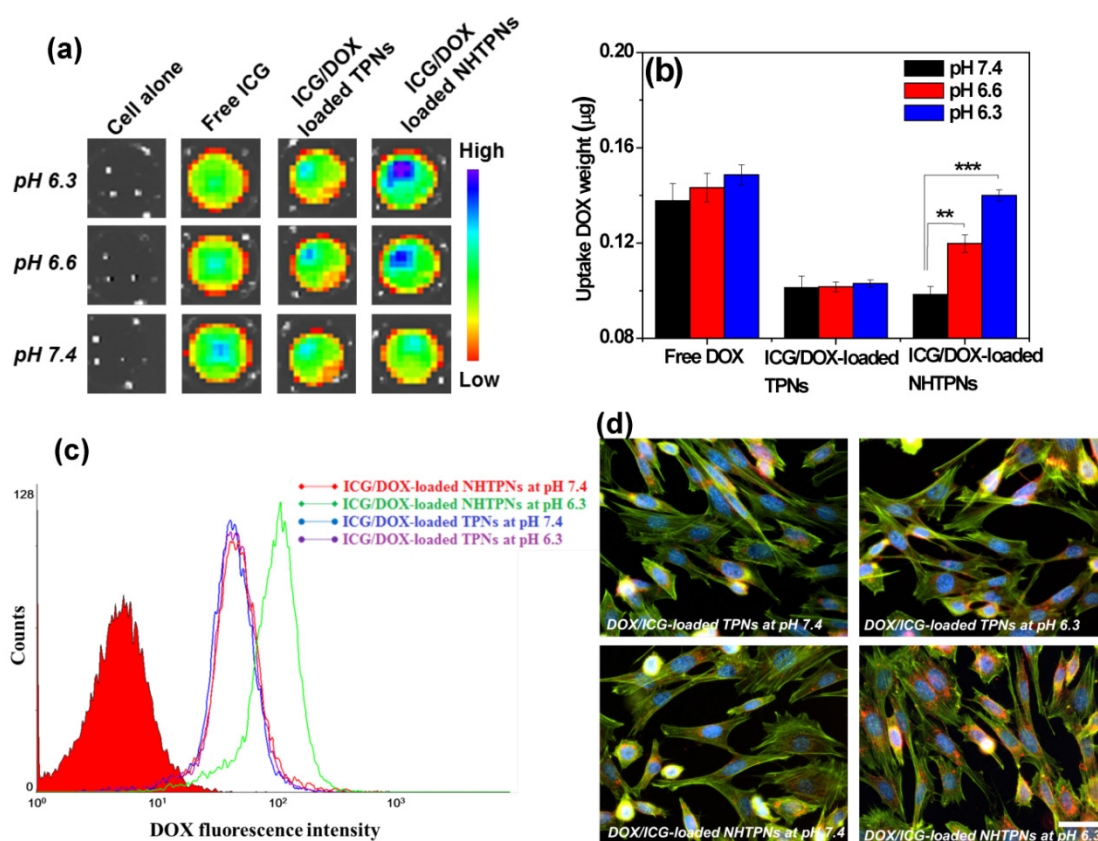


Figure 4. (a) Fluorescence images of ICG molecules from TRAMP-C1 cells incubated with free ICG and ICG/DOX-loaded TPNs and NHTPNs, respectively, under different pH conditions attained by IVIS. (b) Intracellular DOX amount of TRAMP-C1 cells incubated with various DOX formulations. (c) Flow cytometric histograms TRAMP-C1 cells treated with ICG/DOX-loaded TPNs and NHTPNs at pH 7.4 and 6.3 for 2 h (DOX concentration = 20 μM). (d) Fluorescence images of TRAMP-C1 cells incubated with ICG/DOX-loaded TPN and NHTPNs at pH 7.4 and 6.3 for 1.5 h (DOX concentration = 10 μM). Nuclei and F-actin cytoskeleton were stained with Hoechst and F-actin marker, respectively. Scale bar is 50 μm .

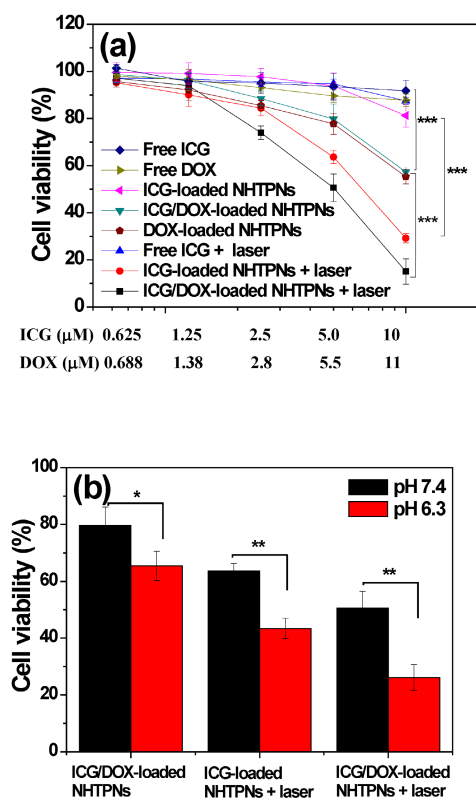


Figure 5. (a) Cell viability of TRAMP-C1 cells incubated with various formulations for 24 h with and without the 5-min NIR laser irradiation, followed by additional 24 h incubation. (b) Cell viability of TRAMP-C1 cells incubated respectively with ICG-loaded NHTPNs and ICG/DOX-loaded NHTPNs (ICG 5.0 μM and DOX 5.5 μM , if applicable) at pH 7.4 and 6.3.

Moreover, in the absence of NIR laser irradiation, the comparable cytotoxicity of ICG/DOX-loaded NHTPNs against TRAMP-C1 cells to DOX-loaded NHTPNs indicates that the presence of ICG has little influence on cancer chemotherapy efficacy of DOX released from NHTPNs. With NIR irradiation, the ICG/DOX-loaded NHTPNs showed the highest efficacy in inhibiting the proliferation of TRAMP-C1 cells by combined photothermal/chemo therapy. On the other hand, as revealed in Figure 5b, after NIR laser irradiation, the viability of TRAMP-C1 cells incubated respectively with ICG/DOX-loaded NHTPNs and ICG-loaded NHTPNs at pH 6.3 was appreciably reduced compared to the cells treated at pH 7.4. In the absence of NIR laser irradiation, the enhanced cytotoxicity of ICG/DOX-loaded NHTPNs in response to the change of culture pH from 7.4 to 6.3 was also observed. The results clearly demonstrate the promotion of anticancer effect from payload-containing NHTPNs by virtue of the increased intracellular concentrations of therapeutic agents upon acid-activated cellular uptake.

In Vivo Imaging and Biodistribution Analysis

The effects of the pH_e -responsive surface charge transition of cargo-loaded NHTPNs on in vivo tumor

accumulation and biodistribution were further evaluated using the subcutaneous TRAMP-C1 tumor model in male C57BL/6J mice. The ICG/DOX-loaded TPNs which lacked NAcHis elaboration were used as the control. Upon intravenous injections with various nanoparticles loaded with either ICG alone or both ICG/DOX, the cargo accumulation in tumor regions of the tumor-bearing mice was examined by intravital ICG fluorescence imaging. Compared to the weak fluorescence signal in the tumor regions of the free ICG group at 6 h post-injection, the intense fluorescence signals of the NHTPN and TPN groups over the identical time period were detected (Figure 6a). The signals lasted even for 48 h after injection. This demonstrates the pronounced ability of NHTPNs and TPNs in promoting their accumulation in tumor areas by virtue of the EPR effect and in protecting ICG from degradation and body clearance. It should be noted that the ICG fluorescence intensities at the tumor sites of the two NHTPN groups were appreciably higher than that of the TPN group over the time course.

The ex vivo NIR fluorescence signal of tumor receiving free ICG was not detected at 48 h post-injection, while the tumors from the NHTPN groups with the loaded cargo of either ICG alone or ICG/DOX exhibited higher fluorescence intensities than that from the group receiving the ICG/DOX-loaded TPNs (Figure 6b and c). Since the particle sizes of the ICG/DOX-loaded NHTPNs and TPNs were essentially identical (ca 50 nm in D_h as shown in Table 1), the significantly enhanced tumor accumulation of the former is attributed to the increased surface positive charges from protonation of NAcHis (imidazole) residues by the tumor extracellular acidity. This is consistent with the biodistribution profiles of the NHTPNs carrying ICG/DOX (Figure 6b and c), showing that the ex vivo ICG fluorescence intensity was higher in tumor than that in liver. Similar biodistribution of ICG delivered by functionalized nanocarriers has been attained [30,31]. By contrast, owing to the reduced tumor uptake by the lack of NAcHis residues, an appreciably enhanced accumulation of cargo-loaded TPNs in liver rather than in tumor was observed. These results indicate that the NHTPNs can greatly promote the tumor-targeted delivery of ICG and DOX, thus holding promise for improved cancer theranosis. Furthermore, the slightly increased tumor accumulation of ICG/DOX-loaded NHTPNs compared to ICG-loaded NHTPNs was attributed to the small particle size (Figure 1a) and the nearly neutral surfaces of ICG/DOX-loaded NHTPNs (Figure 3a) in tumor weak acidic environment which promote their tumor uptake upon the enhanced penetration ability and affinity with cancer cells.

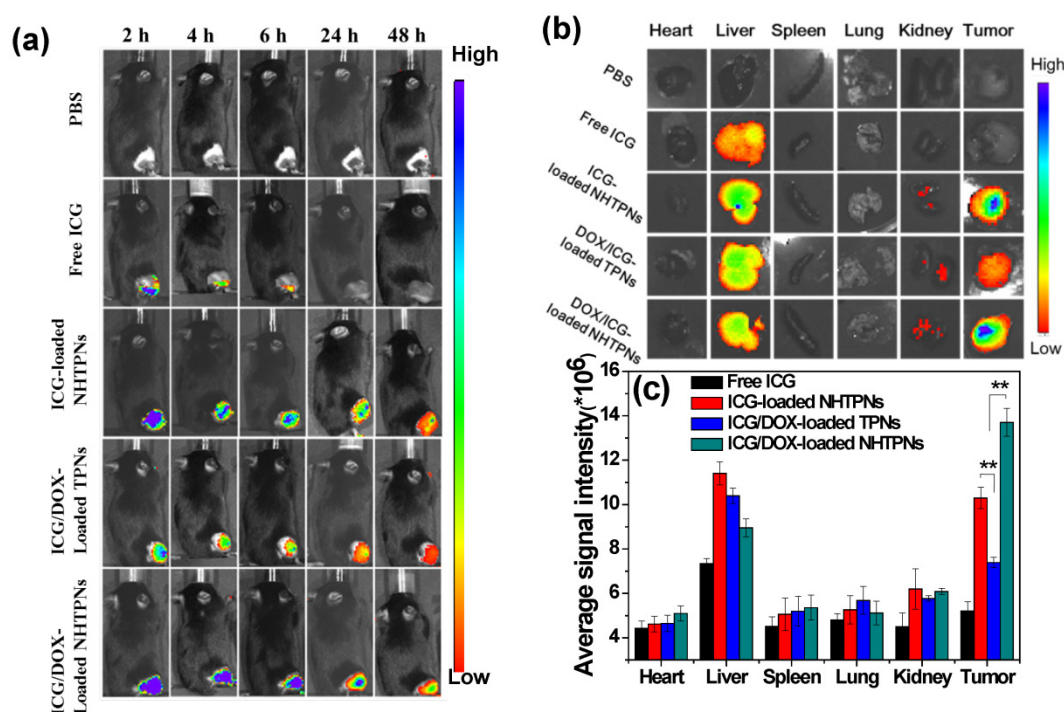


Figure 6. (a) In vivo NIR fluorescence images of TRAMP-C1 tumor-bearing mice receiving intravenous injection of PBS and different ICG-containing formulations evaluated by IVIS. (b) NIR fluorescence images of the isolated major organs and tumors 48 h post-injection with PBS and different ICG-containing formulations. (c) Average ICG fluorescence intensities of individual organs and tumor from TRAMP-C1 tumor-bearing mice treated with different ICG-containing formulations (n = 5 per group).

Intratumoral Distribution

To assess the tumor penetration ability of cargo-carrying nanoparticles, their intratumoral distribution was attained by IHC staining of tumor tissue sections. The tumors receiving the ICG/DOX-loaded NHTPNs and TPNs exhibited appreciably higher DOX fluorescence intensity than that receiving free DOX regardless of NIR irradiation (Figure 7a), further illustrating the superior tumor accumulation of the nanoformulations via the EPR effect. The DOX fluorescence signal from the ICG/DOX-loaded NHTPN treatment was more intense within tumor and farther in distance from the CD31-identified tumor blood vessels than that treated with the TPN counterpart, suggesting that the extravasated NHTPNs from tumor neovessels were substantially uptaken by cancer cells and, for the rest not internalized by cancer cells, readily penetrated into the deep cell-dense tumor region due to their small size and p*H*_e-induced near-neutral surface. By contrast, the TPNs were localized mostly in the vessel periphery due to their negative charge-rich surfaces which impeded tumor uptake and permeation [35,36]. The DOX fluorescence intensity was significantly enhanced when tumors treated with ICG/DOX-loaded NHTPNs and TPNs were subjected to additional NIR irradiation, because the photo-triggered hyperthermia could not only disrupts the dense tumor extracellular matrix but also promote the permeability of tumor angiogenic ves-

sels, thus facilitating tumor accumulation of nanoparticles. Similar viewpoints have also been reported elsewhere [41,42].

Although we have confirmed the deep tumor penetration of NHTPNs, whether the payload-carrying NHTPNs can further infiltrate into deep tumor hypoxia regions, with a weak acidic microenvironment of ca pH 6.0 and a distance as far as 150 μm from the neovessels, needs to be verified [22,43]. As shown in Figure 7b, the localization of ICG/DOX-loaded NHTPNs within the HIF 1α positive areas implies the presence of NHTPNs in the deep tumor hypoxia. The HIF 1α-identified tumor hypoxia correlated well with the contiguous tumor section stained with a CD11b marker, suggesting that the transport of NHTPNs from vessel periphery into tumor hypoxia may involve cellular cargo pickup via the hypoxia-homing recruitment of TAMs [36, 44-47]. By contrast, the access of ICG/DOX-loaded TPNs and free DOX to tumor hypoxia was severely restricted (Figure 7c). It was further postulated that the difference in accessibility of tumor hypoxia to the two nanoparticles as observed in Figure S6 was caused predominantly by the increased surface positive charges of NHTPNs in the tumor acidic microenvironment and thus the cellular midway uptake by TAMs. The results of in vitro cellular uptake study using RAW 264.7 cells (mouse leukemic monocyte macrophage cell line) show a dramatic enhancement in ICG fluorescence intensity for RAW 264.7 cells incubated with

cargo-loaded NHTPNs with medium pH adjustment from pH 7.4 to 6.3 (Figure S7), compared with only a limited increase in ICG fluorescence intensity for the cells treated with the TPN counterpart. As postulated, the acidity-triggered surface charge conversion of

NHTPNs indeed facilitated their uptake by macrophages. The enhanced internalization of free ICG by RAW 264.7 cells at pH 7.4 (Figure S7) was a result of extensive self-aggregation that facilitated the phagocytic uptake.

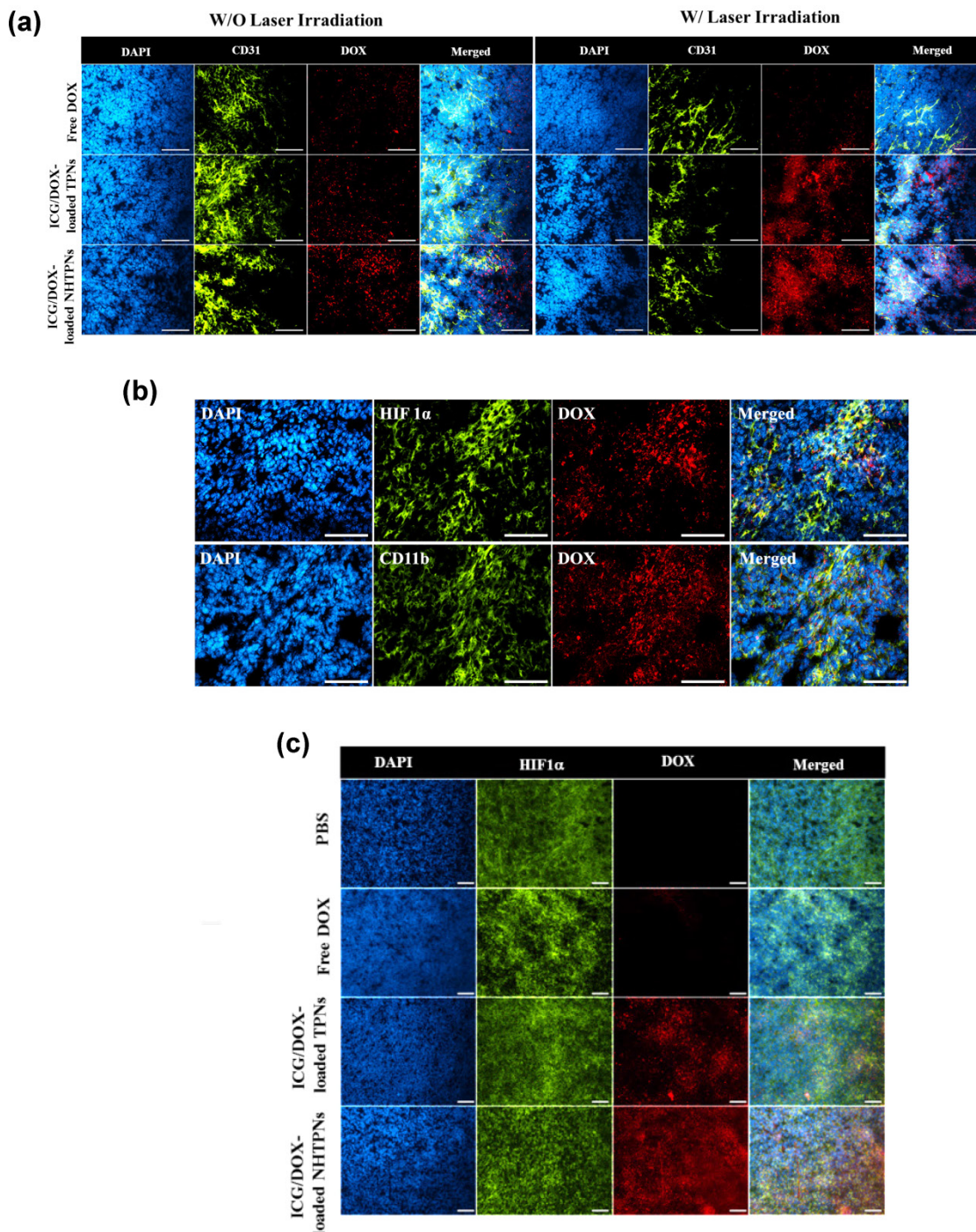


Figure 7. (a) Intratumoral distribution of free DOX and ICG/DOX-loaded TPNs and NHTPNs in relation to the loci of angiogenic blood vessels examined by immunofluorescence microscopy. (b) Intratumoral distribution of ICG/DOX-loaded NHTPNs in relation to the loci of tumor hypoxia and TAM by IHC examination of contiguous tumor sections. (c) Intratumoral distribution of free DOX and ICG/DOX-loaded TPNs and NHTPNs in relation to the loci of tumor hypoxia examined by immunofluorescence microscopy. Tumor cell nuclei, angiogenic blood vessels, tumor hypoxia and TAM were stained with DAPI and CD31, HIF 1α and CD11b markers, respectively. Scale bars are 50 μm in (a) and 100 μm in (b and c).

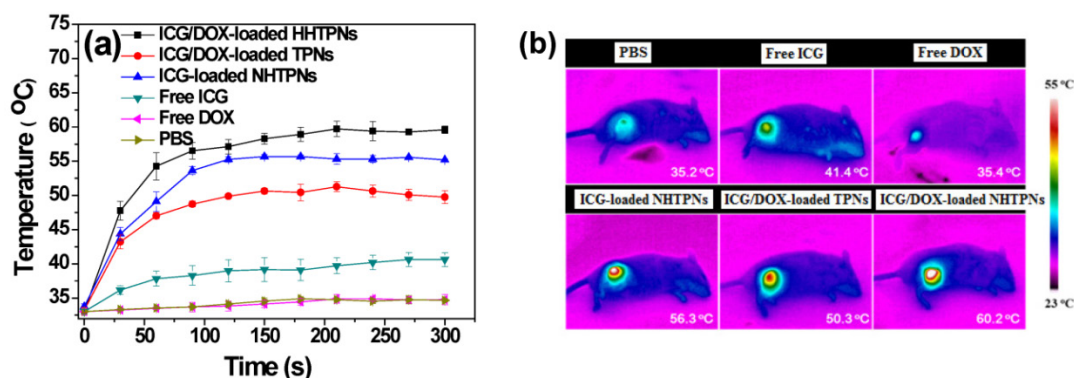


Figure 8. (a) Temperature profiles and (b) infrared thermographic maps at the tumor sites of TRAMP-C1 tumor-bearing mice receiving various formulations and exposed to NIR laser irradiation of 1.0 W/cm² 6 h post-injection.

In Vivo Tumor Growth Inhibition by the Imaging-Guided Photothermal/Chemobiotherapeutic Therapy

Due to the enhanced accumulation of ICG-containing NHTPNs and TPNs at TRAMP-C1 tumor sites via the EPR effect (Figure 6), a significant rise in local tumor temperature upon NIR laser irradiation (1.0 W/cm²) at 6 h post-injection was observed (Figure 8). Because of the low intratumoral ICG concentration, the tumor temperature of free ICG-treated mice under NIR irradiation was only slightly higher than that of the control group injected with either free DOX or PBS. Notably, compared to all other ICG-containing formulations, the extensive accumulation of ICG/DOX-carrying NHTPNs in tumor (Figures 6 and 7) led to the most profound NIR-triggered hyperthermia on tumor within which a temperature as high as 60.2 °C was attained (Figure 8). Hyperthermia above 50 °C can readily induce irreversible damage to cancer cells, as reflected by the burning scar at the irradiated tumor sites at day 6 post-treatment (Figure S8). The photo-evolved hyperthermia of ICG- and ICG/DOX-loaded NHTPNs within tumor tissues not only led to extensive cell necrosis, but also prominently induced cell apoptosis, as shown by a remarkable increase in the level of caspase-3 protein, a key molecular indicator for cells undergoing the apoptotic pathway (Figure 9). As reported elsewhere [41, 42, 48], hyperthermia can induce sublethal damages and subsequent apoptosis of cancer cells located in the outer peripheral zones of laser-irradiated tumor sites, in addition to the increased blood flow which, in turn, can further facilitate the tumor accumulation of therapeutic nanoparticles.

The in vivo antitumor efficacies of various formulations in terms of the change of tumor volume of the TRAMP-C1 tumor-bearing mice were evaluated for up to 15 days post intravenous injection. Little change in body weight of the treated mice over time

in all groups was observed, revealing that the formulations adopted in this study did not induce severe acute toxicity (Figure S9). The tumor volumes (V) were normalized against their original volumes (V_0) to obtain the relative tumor volumes (V/V_0). As shown in Figure 10a, 15 days after treatment, a 22~26-fold increase in the relative tumor volume of mice treated with either free DOX or ICG with laser irradiation was observed, indicating the failure of tumor growth inhibition due to poor tumor accumulation of ICG and DOX. By contrast, the administration of NHTPNs loaded with either ICG alone or ICG/DOX combined with laser irradiation led to an appreciable suppression on tumor growth up to 7 days post injection, beyond which tumors treated with ICG-loaded NHTPNs gradually enlarged, due to the proliferation of residual cells surviving the single-dose photothermal therapy. For the group treated with ICG/DOX-loaded NHTPNs without irradiation, the single DOX chemotherapy was incapable of inhibiting tumor growth. By combining the NIR-triggered hyperthermia and DOX chemotherapy, nevertheless, the ICG/DOX-loaded NHTPNs significantly retarded tumor growth with only a slight tumor recurrence at the end of treatment. On the other hand, the dual-modality therapy delivered by TPNs failed to effectively inhibit tumor growth due to its poor tumor accumulation and cellular uptake, as demonstrated in Figures 6 and 7. Based on the superior performances of ICG/DOX-loaded NHTPNs in intratumoral distribution and tumor growth inhibition, it is concluded that the photo-evolved hyperthermia not only induces effective thermal ablation of cancer cells but also promotes DOX penetration throughout the tumor, thus substantially inhibiting cancer cell proliferation.

In agreement with the results of the in vivo tumor growth inhibition, tumors harvested from the sacrificed mice receiving ICG/DOX-loaded NHTPNs and NIR irradiation were the smallest among the tumors receiving other treatments (Figure 10a). As

shown in Table S1, the average TI (ca 73.5 %) of the combinatorial therapy provided by ICG/DOX-loaded NHTPNs with NIR activation was appreciably higher than that without NIR irradiation (26.9 %) and that of ICG/DOX-loaded TPNs with NIR illumination (30.3 %). This further demonstrates that the dual-modality therapy delivered by ICG/DOX-loaded NHTPNs exhibited the highest antitumor efficacy. As illustrated by H&E staining of the tumor sections (Figure 10b), TRAMP-C1 tumor tissue receiving PBS and laser irradiation showed the same histologic features compared to the group without illumination, indicating that the NIR irradiation (1 W/cm²) by itself was essentially harmless to the tissue. Tumors treated with either free ICG or DOX along with laser irradiation showed no apparent tissue damage primarily because of the lack of tumor targeting and thus the low drug accumulation in tumors. Upon laser irradiation, tumors receiving ICG/DOX-loaded NHTPNs exhibited more severe cell necrosis and extensive hemorrhagic inflammation as compared to those treated with either ICG/DOX-loaded TPNs or ICG-loaded NHTPNs.

Compared to the ICG-loaded NHTPN treatment, the damage to tumor tissue receiving ICG/DOX-loaded NHTPNs was significantly enhanced, thereby clearly demonstrating the therapeutic effect of the chemotherapy, most likely with the aid of photo-triggered hyperthermia in enhancing DOX penetration into deep tumor tissue and in accelerating PLGA degradation. Upon the treatment with the photothermal therapy from ICG-loaded NHTPNs, the H&E examination of tumor sections showed only sporadic necrotic regions along with occasional appearances of pyknosis. No apparent abnormality was observed in major organs, particularly in liver of mice treated with all nanoformulations, because the NIR irradiation as a hyperthermia trigger was applied exclusively on tumors only (Figure S10). These results strongly suggest that the imaging-guided photothermal/chemo combinatorial therapy of ICG/DOX-loaded NHTPNs developed herein not only can significantly reduce side effects on normal tissues, but also display a sound anti-tumor efficacy.

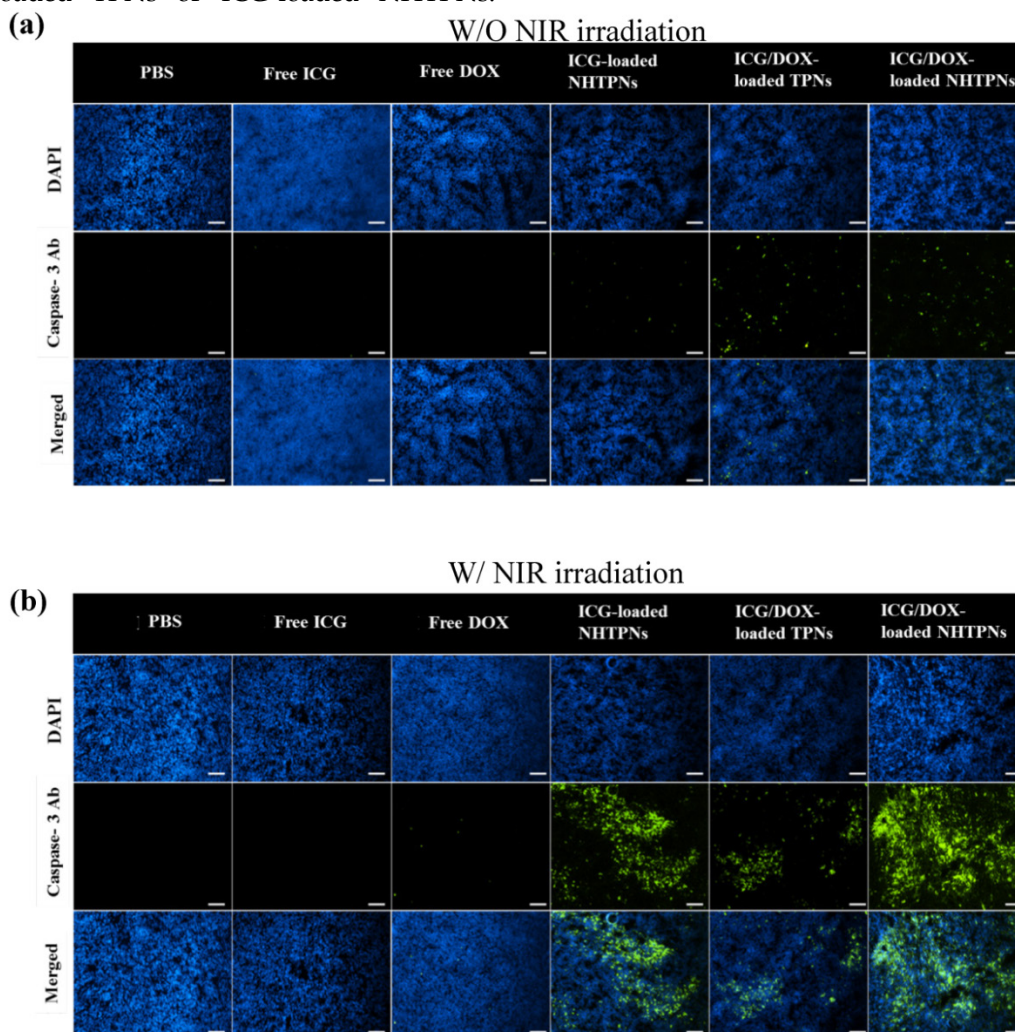


Figure 9. Fluorescence images of tumor sections from the mice bearing TRAMP-C1 tumor 48 h post-injection of various formulations (a) without and (b) with NIR irradiation. Cell nuclei and apoptotic cells were stained with DAPI (blue) and caspase-3 marker (green), respectively. Scale bars are 100 μ m.

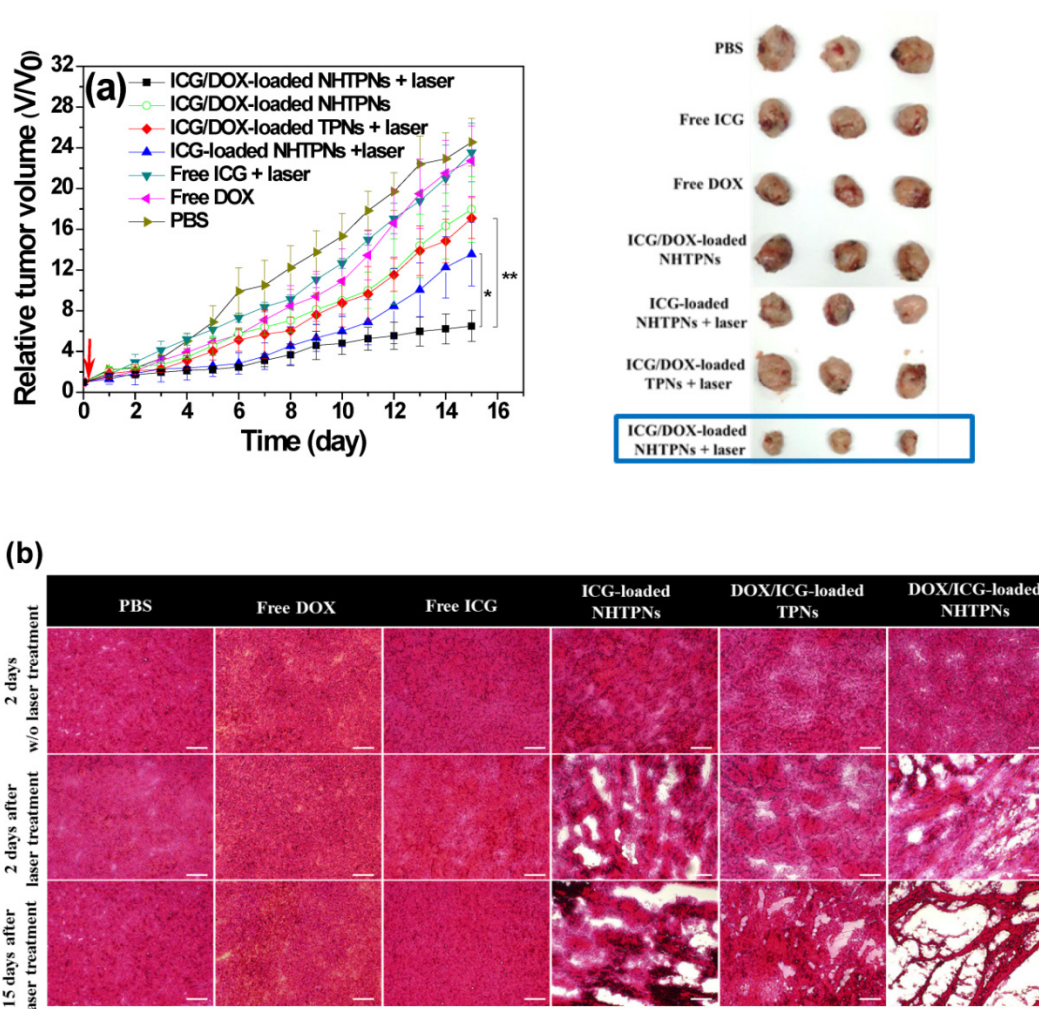


Figure 10. (a) Tumor growth inhibition profiles of the mice bearing TRAMP-C1 tumor injected with various formulations, followed by NIR laser irradiation (5 min, 1.0 W/cm²) 6 h post-injection or without any laser treatment (n = 4 per group). Morphology and size of the tumors of each group isolated from the sacrificed mice at day 15 (the end point) after the treatment. (b) Images of H&E-stained tumor sections harvested from the tumor-bearing mice receiving treatments. Scale bars are 100 μm.

Conclusions

To improve the efficacy of cancer treatment by combined photothermal/chemo therapy, the pH_e-responsive surface charge switchable nanocarriers comprising hydrophobic PLGA cores and NA-Chis-TPGS coating were developed to selectively transport ICG and DOX. The physiochemical and in vitro cellular uptake patterns suggest that the ICG/DOX-loaded NHTPNs can greatly promote the uptake of cargos by TRAMP-C1 and MCF-7 cancer cells as well as macrophage-like RAW 264.7 cells under weak acidic conditions by means of their enhanced attraction with the negatively-charged cell membrane surfaces, due to the increased protonation of the NAChis (imidazole) residues on particle surfaces. The results of in vivo and ex vivo biodistribution studies further reveal that the payload-carrying NHTPNs not only substantially accumulated within TRAMP-C1 solid tumor but also actively penetrated

into deep tumor hypoxia by virtue of their pH_e-triggered near neutral surfaces and the additional hitchhiking transport via TAMs. The results of in vivo animal study demonstrates the sound imaging-guided photothermal effects of ICG/DOX-loaded NHTPNs on inducing extensive cell necrosis and apoptosis and enhancing additional DOX chemotherapy, thereby prominently inhibiting tumor growth and recurrence. Over all, the ICG/DOX-loaded NHTPNs featured with a superior tumor accumulation/uptake and photothermal/chemo dual-modality therapy show great promise in improving cancer theranosis.

Supplementary Material

Figures S1-10 and Table S1.
<http://www.thno.org/v06p0302s1.pdf>

Acknowledgements

This work is supported by the Ministry of Sci-

ence and Technology, Taiwan (MOST 102-2221-E-007-032-MY3, 102-2221-E-007-133-MY3 and 103-2221-E-007-023) and National Tsing Hua University, Taiwan (104N2046E1 and 104N2742E1).

Competing Interests

The authors have declared that no competing interest exists.

References

- Mura S, Nicolas J, Couvreur P. Stimuli-responsive nanocarriers for drug delivery. *Nat. Mater.* 2013; 12: 991-1003.
- Cabral H, Nishiyama N, Kataoka K. Supramolecular nanodevices: from design validation to theranostic nanomedicine. *Acc. Chem. Res.* 2011; 44: 999-1008.
- Gao GH, Li Y, Lee DS. Environmental pH-sensitive polymeric micelles for cancer diagnosis and targeted therapy. *J. Controlled Release.* 2013; 169: 180-4.
- Zhen Z, Tang W, Chuang YJ, Todd T, Zhang W, Lin X, Niu G, Liu G, Wang L, Pan Z, Chen X, Xie J. Tumor vasculature targeted photodynamic therapy for enhanced delivery of nanoparticles. *ACS Nano.* 2014; 8: 6004-13.
- Gong H, Dong Z, Liu Y, Yin S, Cheng L, Xi W, Xiang J, Liu K, Li Y, Liu Z. Engineering of multifunctional nano-micelles for combined photothermal and photodynamic therapy under the guidance of multimodal imaging. *Adv. Funct. Mater.* 2014; 24: 6492-6502.
- Chiang WH, Huang WC, Chang CW, Shen MY, Shih ZF, Huang YF, Lin SC, Chiu HC. Functionalized polymeric micelles with outlayered polyelectrolyte gels for potential tumor-targeted delivery of multimodal therapies and MR imaging. *J. Controlled Release.* 2013; 168: 280-8.
- Xuan M, Shao J, Lin X, Dai L, He Q. Self-propelled Janus mesoporous silica nanomotors with sub-100 nm diameters for drug encapsulation and delivery. *Chemphyschem.* 2014; 15: 2255-60.
- Xuan M, Shao J, Dai L, He Q, Li J. Macrophage cell membrane camouflaged mesoporous silica nanocapsules for in vivo cancer therapy. *Adv. Healthc. Mater.* 2015; 4: 1645-52.
- Wang J, Sun X, Mao W, Sun W, Tang J, Sui M, Shen Y, Gu Z. Tumor redox heterogeneity-responsive prodrug nanocapsules for cancer chemotherapy. *Adv. Mater.* 2013; 25: 3670-6.
- Li YL, Zhu L, Liu Z, Cheng R, Meng F, Cui JH, Ji SJ, Zhong Z. Reversibly stabilized multifunctional dextran nanoparticles efficiently deliver doxorubicin into the nuclei of cancer cells. *Angew. Chem. Int. Ed.* 2009; 48: 9914-8.
- Dai J, Lin S, Cheng D, Zou S, Shuai X. Interlayer-crosslinked micelle with partially hydrated core showing reduction and pH dual sensitivity for pin-pointed intracellular drug release. *Angew. Chem. Int. Ed.* 2011; 50: 9404-8.
- Gratton SE, Ropp PA, Pohlhaus PD, Luft JC, Madden VJ, Napier ME, DeSimone JM. The effect of particle design on cellular internalization pathways. *Proc. Natl. Acad. Sci. USA* 2008; 105: 11613-8.
- Vader P, Aa LJ, Engbersen JF, Storm G, Schiffelers RM. Physicochemical and biological evaluation of siRNA polyplexes based on PEGylated poly(amido amine)s. *Pharm. Res.* 2012; 29: 352-61.
- Shao J, Xuan M, Dai L, Si T, Li J, He Q. Near-Infrared-Activated Nanocalorifiers in Microcapsules: Vapor Bubble Generation for In Vivo Enhanced Cancer Therapy. *Angew. Chem. Int. Ed.* 2015; 54: 12782-7.
- Breus VV, Heyes CD, Tron K, Nienhaus GU. Zwitterionic biocompatible quantum dots for wide pH stability and weak nonspecific binding to cells. *ACS Nano.* 2009; 3: 2573-80.
- Muro E, Pons T, Lequeux N, Fragola A, Sanson N, Lenkei Z, Dubertret B. Small and stable sulfobetaine zwitterionic quantum dots for functional live-cell imaging. *J. Am. Chem. Soc.* 2010; 132: 4556-7.
- Arvizo RR, Miranda OR, Moyano DF, Walden CA, Giri K, Bhattacharya R, Robertson J D, Rotello VM, Reid JM, Mukherjee P. Modulating pharmacokinetics, tumor uptake and biodistribution by engineered nanoparticles. *PLoS One.* 2011; 6: e24374.
- Alexis F, Pridgen E, Molnar LK, Farokhzad OC. Factors affecting the clearance and biodistribution of polymeric nanoparticles. *Mol. Pharm.* 2008; 5: 505-15.
- Du JZ, Sun TM, Song WJ, Wu J, Wang J. A tumor-acidity-activated charge-conversional nanogel as an intelligent vehicle for promoted tumoral-cell uptake and drug delivery. *Angew. Chem. Int. Ed.* 2010; 49: 3621-6.
- Yuan YY, Mao CQ, Du XJ, Du JZ, Wang F, Wang J. Surface charge switchable nanoparticles based on zwitterionic polymer for enhanced drug delivery to tumor. *Adv. Mater.* 2012; 24: 5476-80.
- Hu J, Miura S, Na K, Bae YH. pH-Responsive and charge shielded cationic micelle of poly(L-histidine)-block-short branched PEI for acidic cancer treatment. *J. Controlled Release.* 2013; 172: 69-76.
- Dreaden EC, Morton SW, Shopsowitz KE, Choi JH, Deng ZJ, Cho NJ, Hammond PT. Bimodal tumor-targeting from microenvironment responsive hyaluronan layer-by-layer (LbL) nanoparticles. *ACS Nano.* 2014; 8: 8374-82.
- Zhang Y, Wang C, Xu C, Yang C, Zhang Z, Yan H, Liu K. Morpholino-decorated long circulating polymeric micelles with the function of surface charge transition triggered by pH changes. *Chem. Commun.* 2013; 49: 7286-8.
- Poon Z, Chang D, Zhao X, Hammond PT. Layer-by-layer nanoparticles with a pH-sheddable layer for in vivo targeting of tumor hypoxia. *ACS Nano.* 2011; 5: 4284-92.
- Mo R, Sun Q, Xue J, Li N, Li W, Zhang C, Ping Q. Multistage pH-responsive liposomes for mitochondrial-targeted anticancer drug delivery. *Adv. Mater.* 2012; 24: 3659-65.
- Guana X, Li Y, Jiao Z, Chen J, Guo Z, Tian H, Chen X. A pH-sensitive charge-conversion system for doxorubicin delivery. *Acta Biomater.* 2013; 9: 7672-8.
- Hu X, Guan X, Li J, Pei Q, Liu M, Xie Z, Jing X. Hybrid polymer micelles capable of cRGD targeting and pH-triggered surface charge conversion for tumor selective accumulation and promoted uptake. *Chem. Commun.* 2014; 50: 9188-91.
- Zan M, Li J, Luo S, Ge Z. Dual pH-triggered multistage drug delivery systems based on host-guest interaction-associated polymeric nanogels. *Chem. Commun.* 2014; 50: 7824-7.
- Lee ES, Shin HJ, Na K, Bae YH. Poly(L-histidine)-PEG block copolymer micelles and pH-induced destabilization. *J. Controlled Release.* 2003; 90: 363-74.
- Wan Z, Mao H, Guo M, Li Y, Zhu A, Yang H, He H, Shen J, Zhou L, Jiang Z, Ge C, Chen X, Yang X, Liu G, Chen H. Highly efficient hierarchical micelles integrating photothermal therapy and singlet oxygen-synergized chemotherapy for cancer eradication. *Theranostics.* 2014; 4: 399-411.
- Zheng M, Zhao P, Luo Z, Gong P, Zheng C, Zhang P, Yue C, Gao D, Ma Y, Cai L. Robust ICG theranostic nanoparticles for folate targeted cancer imaging and highly effective photothermal therapy. *ACS Appl. Mater. Interfaces.* 2014; 6: 6709-16.
- Zheng X, Zhou F, Wu B, Chen WR, Xing D. Enhanced tumor treatment using biofunctional indocyanine green-containing nanostructure by intratumoral or intravenous injection. *Mol. Pharm.* 2012; 9: 514-22.
- Jian WH, Yu TW, Chen CJ, Huang WC, Chiu HC, Chiang WH. Indocyanine Green-Encapsulated Hybrid Polymeric Nanomicelles for Photothermal Cancer Therapy. *Langmuir.* 2015; 31: 6202-10.
- Nomura T, Koreeda N, Yamashita F, Takakura Y, Hashida M. Effect of particle size and charge on the disposition of lipid carriers after intratumoral injection into tissue-isolated tumors. *Pharm. Res.* 1998; 15: 128-32.
- Lieleg O, Baumgärtel RM, Bausch AR. Selective filtering of particles by the extracellular matrix: an electrostatic bandpass. *Biophys. J.* 2009; 97: 1569-77.
- Ernsting MJ, Murakami M, Roy A, Li SD. Factors controlling the pharmacokinetics, biodistribution and intratumoral penetration of nanoparticles. *J. Controlled Release.* 2013; 172: 782-94.
- Xu X, Li Y, Li H, Liu R, Sheng M, He B, Gu Z. Smart nanovehicles based on pH-triggered disassembly of supramolecular peptide-amphiphiles for efficient intracellular drug delivery. *Small.* 2014; 10: 1133-40.
- Chiang WH, Huang WC, Shen MY, Wang CH, Huang YF, Lin SC, Chern CS, Chiu HC. Dual-layered nanogel-coated hollow lipid/polypeptide conjugate assemblies for potential pH-triggered intracellular drug release. *PLoS One.* 2014; 9: e92268.
- Chiang WH, Ho VT, Huang WC, Huang YF, Chern CS, Hsin-Cheng Chiu. Dual stimuli-responsive polymeric hollow nanogels designed as carriers for intracellular triggered drug release. *Langmuir.* 2012; 28: 15056-64.
- Chiang WH, Ho VT, Chen HH, Huang WC, Huang YF, Lin SC, Chern CS, Chiu HC. Superparamagnetic hollow hybrid nanogels as a potential guidable vehicle system of stimuli-mediated MR imaging and multiple cancer therapeutics. *Langmuir.* 2013; 29: 6434-43.
- Chu KF, Dupuy DE. Thermal ablation of tumours: biological mechanisms and advances in therapy. *Nat. Rev. Cancer.* 2014; 14: 199-208.
- Kirui DK, Koay EJ, Guo X, Cristini V, Shen H, Ferrari M. Tumor vascular permeabilization using localized mild hyperthermia to improve macromolecule transport. *Nanomedicine.* 2014; 10: 1487-96.
- Jain RK, Stylianopoulos T. Delivering nanomedicine to solid tumors. *Nat. Rev. Clin. Oncol.* 2010; 7: 653-64.
- Shaffer SA, Baker-Lee C, Kennedy J, Lai MS, de Vries P, Buhler K, Singer JW. In vitro and in vivo metabolism of paclitaxel polyglumex: identification of metabolites and active proteases. *Cancer Chemother. Pharm.* 2007; 59: 537-48.
- Alizadeh D, Zhang L, Hwang J, Schluep T, Badie B. Tumor-associated macrophages are predominant carriers of cyclodextrin-based nanoparticles into gliomas. *Nanomedicine* 2010; 6: 382-90.
- Huang WC, Chiang WH, Cheng YH, Lin WC, Yu CF, Yen CY, Yeh CK, Chern CS, Chiang CS, Chiu HC. Tumor-tropic monocyte-mediated delivery of echogenic polymer bubbles and therapeutic vesicles for chemotherapy of tumor hypoxia. *Biomaterials* 2015; 71: 71-83.
- Huang WC, Shen MY, Chen HH, Lin SC, Chiang WH, Wu PH, Chang CW, Chiang CS, Chiu HC. Monocytic delivery of therapeutic oxygen bubbles for dual-modality treatment of tumor hypoxia. *J. Controlled Release.* 2015; doi: 10.1016/j.jconrel.2015.09.016.
- Yang K, Xu H, Cheng L, Sun C, Wang J, Liu Z. In vitro and in vivo near-infrared photothermal therapy of cancer using polypyrrole organic nanoparticles. *Adv. Mater.* 2012; 24: 5586-92.